GCM gridscale evaporation from mesoscale modelling

J. Noilhan and P. Lacarrère
(Météo-France, CNRM, 31057 Toulouse, France)

November 18, 1991

1 Introduction

Atmospheric general circulation models (GCM) require parameterization of sub-grid scale surface fluxes. Most of current surface schemes in GCM assume horizontally homogeneous landscape conditions althougth these assumptions are rarely met in the real world for horizontal scales up to 100 km. Since the level of complexity in GCM's surface description steadily increases, the aim of this paper is to address the issue of spatial variability in land surface properties from horizontal scales ranging from 10 km, a possible resolution for mesoscale models, to 100 km, the size of a GCM grid box. Many field experiments have been carried out during the last decade to investigate the problem of estimating area-averaged surfaces fluxes over non-homegeneous terrain (HAPEX-MOBILHY 1986 (HM86), FIFE87, EFEDA91,...). From these observations and from mesoscale modelling, it has been shown that spatial changes in surface characteristics affect the overlying atmosphere and, on certain conditions, may generate mesoscale circulations. The effects of surface inhomogeneities on the atmosphere depend on the horizontal scale of landscape variation. Shuttleworth (1988) suggests that for typical length scales less than 10 km, no apparent organisation can be observed in the atmosphere since turbulent processes average everything out. For this type of boundary layer, Mason (1988) and Claussen (1991) showed that at sufficiently large height - the so-called blending height - it is possible to find mean atmospheric conditions in equilibrium with the surface as a whole. Claussen (1991) proposes to estimate the areally averaged surface fluxes at the blending height for each land-use category of a grid box (1 km x 1 km), instead of computing the area fluxes from "effective" surface parameters for the entire area.

On the other land, for horizontal scale of land variations greater than 10 km, mesoscale circulations are generated which affects the whole depth of the boundary layer (Andre et al. 1989, Avissar and Pielke 1989, Bougeault et al. 1991b, Mahfouf et al. 1987, Mascart et al. 1991, Pinty et al. 1989). For this type of boundary layer, the concept of blending height and the Claussen's proposal are no longer valid since the whole vertical structure of the atmosphere

is perturbed by the surface inhomogeneity.

The idea of this paper is to investigate the impact of land surface variability at a scale comparable to the size of a GCM grid box from the numerical results obtained with a mesoscale model, previously validated with the HM86 data set. Our objective is to analyse to what extend one can derive 'effective' parameters for the soil texture and the vegetation in order to compute with a 1D Soil - Vegetation - Atmospheric transfer model an 'area -averaged' flux that supports comparison with the average of the fluxes predicted by the 3D mesoscale model. In the absence of sufficiently detailled observations, even in the HM86 context, the mesoscale model is used as a reference to obtain estimates of averaged fluxes against which the aggregation methods are tested.

Because of the non linear dependence of the surface fluxes on both surface properties and soil water content, estimate of the areally averaged flux from "effective" surface parameters does not necessarily yields the same result as averaging the fluxes themselves.

Such a comparison, if successfully completed, would provide the GCM's modellers with guidelines for averaging surface parameters at a coarser horizontal resolution than existing global classification of soil and vegetation types. The development of aggregation procedures from detailed observations at selected sites to area averages would also provide an essential tool for interpretating the data collected during recent large field experiment (HM86, FIFE 1987, LOTREX 1989, EFEDA 1991, HAPEX-SAHEL 1992,...)

This paper, which focuses on sub-grid scale fluxes over continental area, does not consider :

(i) the effect of the resolved mesoscale fluxes that may be of the same order of magnitude than the sub-grid scale fluxes, at least for calm conditions as shown by Pielke et al. (1991). However, it is important to mention that mesoscale fluxes are significantly reduced when a prevailing wind occurs (Pinty, 1991).

(ii) water, snow and ice surfaces because heat fluxes are governed by quite different physical processes than those over continental areas, which prohibits the definition of effective parameters.

For the purpose of this study, we use a simple parameterization of land suface processes (Noilhan and Planton, 1989 hereafter NP89) which is briefly described in section 2.1 and in the Appendix. The methods for averaging the vegetation properties and the soil texture are presented in sections 2.2 an 2.3, respectively. Section 3 describes the numerical tools used in this study e.g. a mesoscale model (3.1) to provide estimate of the areally averaged suface fluxes, a 1D Atmospheric column model to compute "effective" area surface fluxes when driven by "effective" surface parameters (3.2).

Results of 24 hours integrations and sensitivity studies to the soil and vegetation aggregation methods and to the size of the area considered are discussed in section 4.

Section 5 presents the results of a long term integration ($\sim$ one month) with the 1D model forced by effective parameters representing the whole HM86 experimental area. In this section, we discuss some aspects of the prediction of the mean water content of the soil of a large area, which is a challenge in GCM predictions.

2 Averaging the surface parameters

2.1 The surface parameters in the NP89 scheme

In the NP89 scheme, the number of surface parameters (table 1) has been reduced as much as possible while attempting to preserve the description of the main physical processes. The transfers of heat and water through a superficial and a deep reservoir have been made dependent both upon the soil texture and the soil moisture. The parameters describing the hydraulic and thermal properties (table 2) have been calibrated (C_{gsat}, p, a, C_{2ref}, C_{1sat}) or prescribed ($w_{sat}, w_{fc}, w_{wilt}, b$) from the textural classification of Clapp and Hornberger (1978). Some of these parameters vary more than one decade from coarse to fine soil texture (b, C_{2ref}, C_{1sat}) as a result of large variations in the soil hydraulic conductivity.

A single surface temperature represents the surface energy balance of the land/cover system. The vegetation is described through its horizontal density veg within a grid box, the leaf area index LAI, and a minimum surface resistance R_{smin}. The roughness length Z_0, the albedo α and the emissivity ϵ are related both to the vegetation and to the surface properties. The vegetation intercepts rain, evaporates water retained on the foliage, and transpires.

Most of the surface parameters control indirectly the energy partitioning at the surface. The surface energy balance reads :

$$R_n = H + LE + G$$

where R_n is the net radiation, H the sensible heat flux, LE the latent heat flux and G the soil heat flux. The latent heat flux is the sum of the ground evaporation E_g, the plant transpiration E_{tr} and the evaporation E_r of water intercepted by the foliage :

$$E_g = \frac{veg}{R_a(Z_o)}(h_u q_{sat}(T_s) - q_a)$$

$$E_{tr} = (1 - veg)\frac{(1-\delta)}{R_a(Z_o) + R_s(\frac{R_{smin}}{LAI})}(q_{sat}(T_s) - q_a)$$

$$E_r = (1 - veg)\frac{\delta}{R_a(Z_o)}(q_{sat}(T_s) - q_a)$$

The aerodynamic resistance R_a depends on Z_0, the surface relative humidity h_u on the surface water content w_g. The transpiration is constrained by a surface resistance R_s depending on R_{smin}/LAI and the water w_2 available in the root zone, $q_{sat}(T_s)$ is the saturation specific humidity at the surface temperature T_s and q_a the air specific humidity at the reference level. Jacquemin and Noilhan (1990) have shown that the parameter veg is the most important in the scheme because of its influence on the partitioning of evaporation and on the thermal exchanges at the surface. From the previous expressions and from the equation of T_s (see appendix), we can see that for a fully developed canopy ($veg \rightarrow 1$), plants supply the total evaporation and the soil heat flux becomes negligible. In the absence of water stress and for mild atmospheric conditions, E_{tr} is mainly controlled by the ratio R_{smin}/LAI. The converse is true in the case of bare ground i.e. E_g supplies the total latent heat flux.

2.2 Defining effective parameters for the vegetation

Let us assume that we want to compute area averaged fluxes over a large area, classified into several land use classes for which the fractional area f_i of each land-use category is known, together with its surface properties Z_0^i, veg^i, R_{smin}^i and LAI^i. Spatial averages are computed to obtain effective parameters for the large area. The averaging operators are chosen in order to be consistent with an arithmetic averaging of the fluxes themselves.

- Effective roughness length Z_0^e :

The aerodynamic resistance R_a equals $(C_H U)^{-1}$ where C_H is the drag coefficient and U the wind speed at the first atmospheric model level $Z_b \simeq 20m$.

Averaging C_H over the whole area for neutral conditions yields:

$$C_H = (\frac{k}{ln(\frac{Z_b}{Z_0^e})})^2$$

Where k is the Karman constant, and Z_0^e the effective roughness length. According to Mason (1988) and Claussen (1991), Z_0^e should therefore be defined by :

$$\frac{1}{(ln(\frac{Z_b}{Z_o^e}))^2} = \sum_i f_i \quad \frac{1}{(ln(\frac{Z_b}{Z_o^i}))^2}$$

In the previous expression, the height Z_b is used instead of the blending height, a reasonable approximation if Z_b is sufficiently high.

Another commonly used, more simple evaluation of Z_0^e is :

$$ln(Z_0^e) = \sum_i f_i \quad ln(Z_0^i)$$

These two expressions for Z_o^e have been tested. Because of the low sensitivity of heat flux predictions in NP89 to the roughness length (for variations lower than one decade) (Jacquemin and Noilhan, 1990), the simplest averaging method has been selected.

•The effective minimum surface resistance R_{smin}^e is obtained from :

$$\frac{1}{R_{smin}^e} = \sum_i f_i \quad \frac{1}{R_{smin}^i}$$

Dolman (1991) has studied this type of averaging on the surface conductance, the reciprocal of surface resistance, accounting for spatial variability from an assumed gamma probability distribution. He showed that the effective evaporation flux differed from the areal mean by less than 10%. However, Dolman (1991) noted that the effective evaporation from drier regions was more sensitive to the spatial variability than the evaporation from wetter regions.

• Effective vegetation fraction veg^e, leaf area index LAI^e and albedo α^e :

For this quantities, simple arithmetic means are proposed :

$$veg^e = \sum_i f_i \quad veg^i$$

$$LAI^e = \sum_i f_i \quad LAI^i$$

$$\alpha^e = \sum_i f_i \quad \alpha^i$$

2.3 Defining effective parameters for the soil

The Clapp and Hornberger's relationships describing the hydraulic parameters are based on the most common descriptor of the physical properties, i.e. the soil texture. Using data for 1448 soil samples, Clapp and Hornberger (1978) and Cosby et al. (1984) estimated the standard deviation and the mean for each hydraulic parameter in 11 textural classes using the USDA textural triangle. Using multilinear regression analysis, Cosby et al. (1984) showed that the soil hydraulic characteristics were mainly determined by the particle size distribution : the mean values and the variances of the hydraulic parameters (w_{sat}, K_{sat}, b) were found to be linearly dependent upon the soil texture. Moreover, Cosby et al. showed that most of the variability in soil parameters can be simply related to the sand or clay fractional contents. This result is of great practical importance to map soil parameters in a large area assuming continuous spatial variation in physical properties with respect to sand and clay contents. The forecoming

ideas are adopted to derive the "effective" soil parameters for a large area. As a first step, we performed linear regressions and power law adjustments for each hydraulic parameter (table 2) as a function of both the percent silt and clay contents. These computations were made for the Clapps and Hornberger's parameters (w_{sat}, b) and for the additional NP89's parameters ($C_{gsat}, C_{2ref}, C_{1sat}, p$ and a). The results of this analysis are given in Fig.1. In most of the adjustments, the clay content is found to be a better descriptor than the sand content, except for the saturation volumetric water content w_{sat} (as already shown by Cosby et al.) and C_{gsat}.

These predictive relationships for the thermal-hydraulic parameters are used as long as the fractions of clay and sand are known.

3 Modelling strategy

In this section, we describe the numerical models used to test the methods of aggregation of surface properties. Results obtained from a 3D mesoscale model for several HM86 cases provide the spatial distribution of surface fluxes. These fluxes are used to compute area average at the scale of GCM. A 1D atmospheric column of the same model is then used to compute "effective" surface fluxes using the aggregated parameters and the two results are compared. Both models include the NP89 parameterization, fully interactive with the atmosphere.

3.1 The mesoscale model

The French Weather Service mesoscale model has been used to provide an integration tool and a framework for interpreting experimental results collected during HM86. For this special application, the mesoscale model was run with an enhanced resolution : the horizontal grid mesh was $10km$, the vertical grid had 30 σ levels spaced by approximately $100m$ within the PBL. The simulation domain is a square of about $400km \times 400km$ centered on the HAPEX experimental square and encompassing a fraction of the Pyreneean range. The 3D model includes its usual physical package (radiation, vertical diffusion depending on the turbulent kinetic energy) and the NP89 surface scheme. A detailled description of the implementation of the surface parameterization in the 3D model for the integration on one of the most widely studied period (16 june 86) is given by Bougeault et al. (1988, 1991ab) and Noilhan et al. (1991ab), while integration results concerning the 19 june, 8 july and 10 july 1986 are described by Attié (1990), Giordani (1991) and Noilhan et al. (1991c).

The first step, prior to implementing the surface scheme, was to map the surface parameters over the whole simulation area. A map of soil texture was prepared by Mascart et al. (1988) from several maps of soil available from the literature for the region under study (Fig. 2).

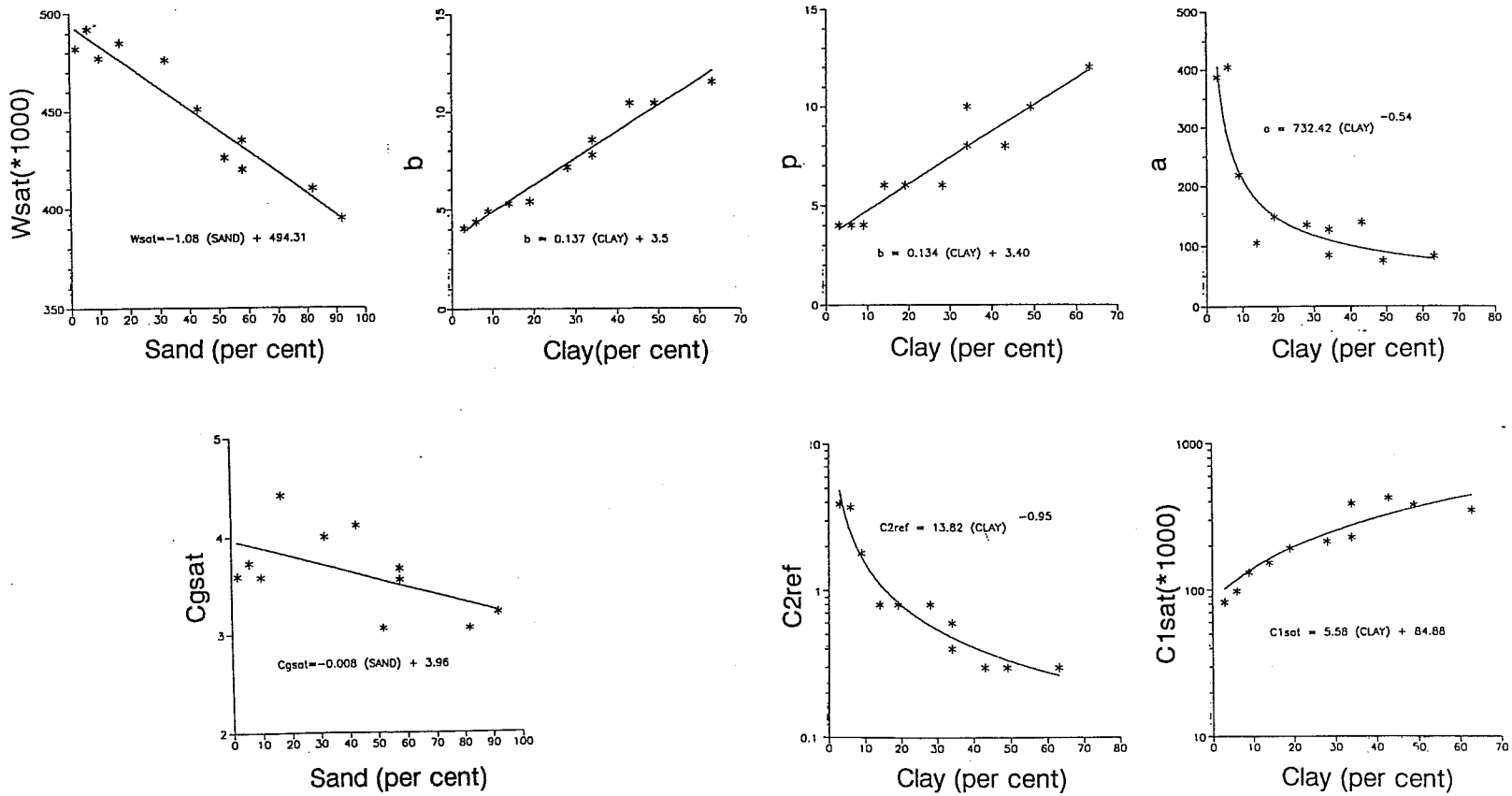

Figure 1a: Plots of the hydraulic parameters (b,a,C_{2ref}, C_{1sat}, w_{sat}, b and C_{gsat})) for each textural class (Table 2) versus the most important variable (percent sand or clay) determined from the regression analysis. The solid line corresponds to the best fit curve given for each parameter.

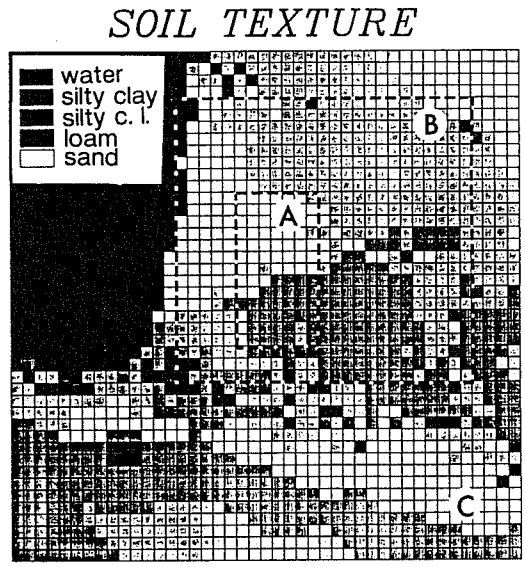

Figure 2: The map of soil textures of Mascart et al. (1988). Present on the map are class 1 (sand), class 5 (loam), class 7 (silty clay loam) and class 10 (silty clay). The target areas A,B and C for testing the aggregation methods are indicated.

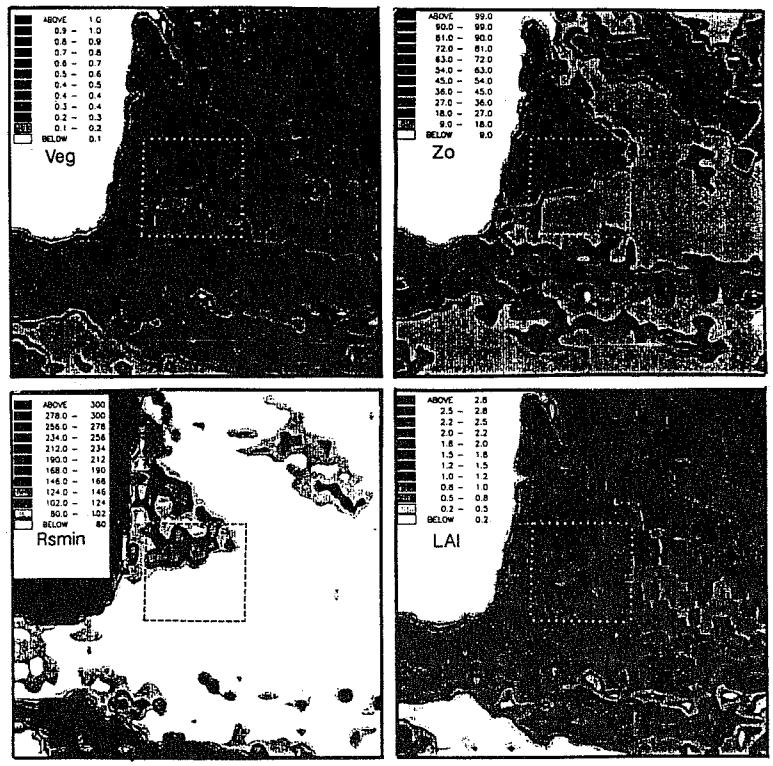

Figure 3: Maps of the model grid scales values of the surface parameters veg, Z_0, R_{smin} and LAI depending upon the vegetation (Phulpin and Noilhan 1989).

The classification is based on the dominant soil texture within each grid box and distinguishes between 4 soil types : sand (1), loam (5), silty clay loam (7) and silty clay (10), where the numbers refer to the original classes of Clapp and Hornberger (1978). The soil parameters are prescribed from this soil map. The strategy for obtaining maps of vegetation parameters was sligtly different, since most of these properties change in time. The data of AVHRR/NOAA6 were processed to obtain a supervised classification of the vegetation type at a scale of about $1km^2$ (Phulpin et al., 1989). After correction of atmospheric effects, two cloud-free NDVI images allowed us to produce a classification of the dominant vegetation type at the AVHRR pixel scale. Seven types of land use were selected: Semi-desert (1), wineyards (2), mediterranean vegetation (3), crops (4), grasslands (5), coniferous (6) and deciduous forests (7). The following method was used to derive maps of surface parameters (Z_o^i, veg^i, R_{smin}^i and LAI^i). We calibrated the NP89 scheme against flux observations at the different measuring sites of HM86 with the 1D model. From this calibration procedure, we assigned values of the scheme parameters to each of the seven vegetation classes. An example of the sets of correspondence obtained on 16 june and 8 july is given in Table 3. The two cases differ mainly by the evolution of the crops, which is characterized by an increase of veg, LAI and Z_0. The minimum stomatal resistance was kept the same for the two cases.

3.2 Examples of mesoscale model results on HM86 cases

Integrations of 24h, starting at $00.00TU$ were performed on three clear days: 16 june, 19 june and 8 july, for which aircraft flux measurements were available over the whole instrumented area. The initial soil water content was prescribed from measurements of soil moisture at 12 sites within the instrumented area.

Detailled comparisons between model results and observations available within a mesoscale sub-domain (domain A) were performed (Noilhan et al., 1991). A description of domain A, corresponding to 7 x 13 model grid boxes, which encompasses a fraction of the Landes forest is given in Fig. 4. Concerning the impact of surface inhomogeneities on the atmosphere, the main striking pattern at the beginning of the observations was the development of a mesoscale circulation between the pine forest and the surrounding crop area. Because its high values of R_{smin} (Gash et al. 1989) and veg (see table 3), the sensible heat flux over the forest was higher than over the crop area both in the observations (André et al., 1988) and in the simulations on 16 and 19 june 1986 (Noilhan et al., 1991 ; Attié, 1990). On the other hand, at the end of the special observing period (after july,1), the contrast between the crops and the forest was reduced as a result of the crop development, resulting in a decrease in the soil heat storage.

These behaviours are illustrated in Fig. 5 showing a comparison between aircraft sensible heat flux estimates close to the surface, and model predictions along the aircraft trajectory on 16, 19 june and 8 july 1986. The general quality of these flux predictions provide the basic validation of the mesoscale integrations on these days. In the following we will use the integrations of 16 june and 8 july to provide a reference for real land use and surface fluxes variability against which the surface aggregation method is tested.

3.3 The 1D model

In the 1D model, large scale advections (horizontal and vertical) are prescribed at each level and interpolated in time from special large scale weather analyses computed every 6 hours during the experiment. The large scale forcing is representative of an area of about $100km \times 100km$ centered on the HM86 central site (see Fig.4). Example of the use of such a 1D model are given by Jacquemin and Noilhan (1990), Mahfouf and Jacquemin (1989), Mahfouf (1990) , Mahfouf and Noilhan (1991).

4 Results of daily integrations

The mesoscale integrations performed on 16 june and 08 july are first used to provide a reference for real land use variability and associated atmospheric predictions for selected target areas.

4.1 Description of target areas

Three mesoscale sub-domains are selected (Fig. 2): The domain A corresponds to the HAPEX instrumented area (Fig. 4), the domain B is an area with terrain height lower than $600m$ and domain C is the entire simulation area, except the portion over the Atlantic ocean. The histograms of soil and vegetation types found in each target area are shown in Fig. 6. One notes that sandy soils are dominant in A, while fine soil textures are dominant in B and C. Concerning the vegetation distribution, the Landes forest is dominant in A. On the other hand, the crops (class 4) and grasslands (class 5) are the most frequent in B and C.

The spatial distribution of the soil types is used to compute effective soil textures for A,B and C from simple arithmetic means:

$$Sand^e = \sum_i f_i \quad Sand^i$$

$$Clay^e = \sum_i f_i \quad Clay^i$$

where $Sand_i$ and $Clay_i$ are the percent composition of each type of soil according to the statistical analysis of Clapp and Hornberger (1978). Given the poor knowledge of the spatial heterogeneity

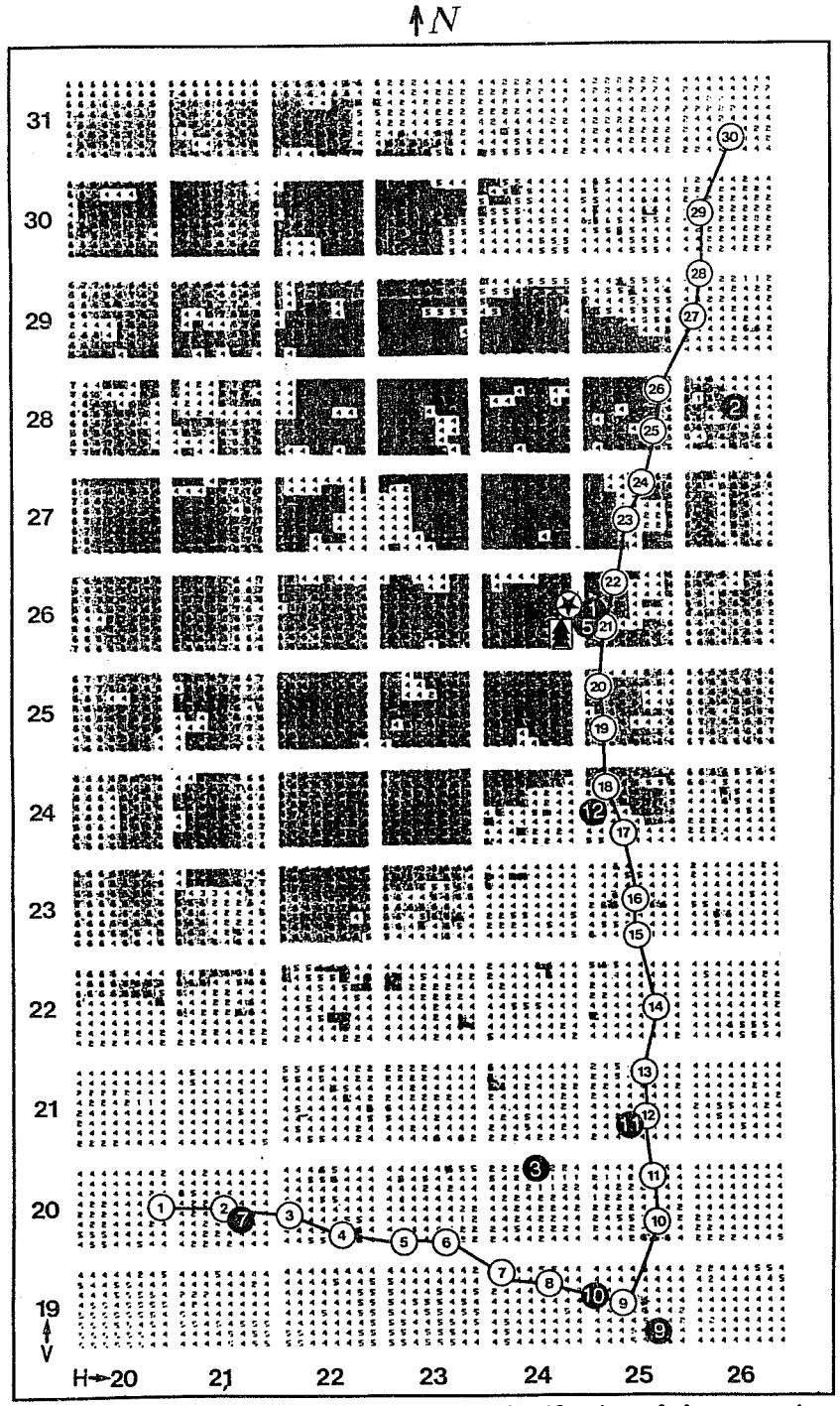

Figure 4 : The mesoscale sub-domain A. The classification of the vegetation at the AVHRR pixel scale is given for each model grid of 10 km x 10 km (2:vineyards, 4:crops, 5: grasslands, 6: coniferous forest, 7: deciduous forest). A model grid includes 64 AVHRR pixels. The solid line indicates the track of the King Air flux measuring aircraft (Hildebrand 1988). The 30 sub-segments along the aircraft leg are given. The surface network includes SAMER stations (full circles) associated with neutron sounding and the HYDRA system (full star) over the Landes forest, near the central site. SAMERS 1 and 5 were installed at the central site where radiosoundings were launched every 2 hours.

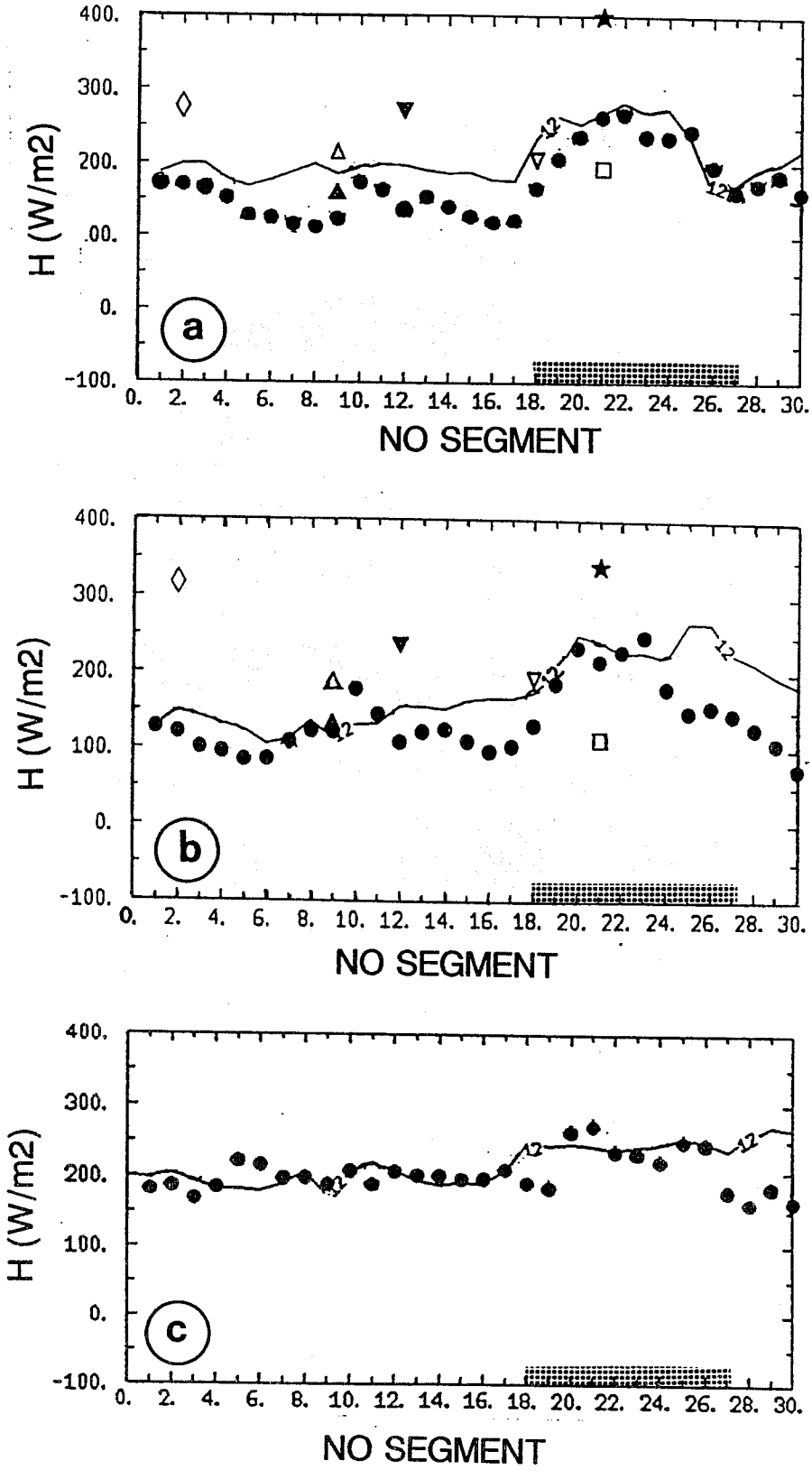

Figure 5: Comparison between the King Air measurements (open circle) and the prediction (full line) of the horizontal variation of the sensible heat flux at 100 m above the surface on 16 june 1986 (a), 19 june 1986 (b) and 10 july 1986 (c).The observations at the SAMER and HYDRA (full star) sites below the aircraft trajectory are reported in (a) and (b). The number in abscissa refer to flight sub-segment numbers (see Fig. 4).

of the soil in the area under study, this crude estimation of the soil texture is attempted as a first guess for testing our aggregation method. Effective parameters for the hydraulic properties are then obtained from the values of $Sand^e$ and $Clay^e$ using the relationships given in Fig.1. The effective soil for A, mainly constituted by classes 1 and 7, corresponds to an intermediate class, close to class number 3 (Fig. 7). Effective soil types for B and C fall within the class of loamy soil, number 5.

4.2 Results of the aggregation procedure

Table 4 summarizes the surface conditions for some of the 1D tests performed for the three domains on 16 june and 08 july. For each ensemble of tests dominant and effective surface properties are alternatively specified. For example, one can see that for test 1, dominant properties are used for domain A (coniferous forest over sandy soil), giving high values for the vegetation properties. Conversely, when averaging the vegetation parameters (test 2), R_{smin} is decreased from $150s/m$ to $66s/m$, the fraction of vegetation from 0.99 to 0.64, the roughness length from $1m$ to $0.38m$ and the leaf area index from 2.3 to 1.7. This pattern is reversed for domains B and C, for which the averaging methods increase the influence of the vegetation, particularly those of the forest. Consequently, the effective vegetation parameters are slightly higher than the dominant properties (crops) in these cases.

- Results for domain A on 16 june 1986

The results obtained for domain A on june 16 are given in Figs. 8 to 10. The mean values and the standard deviations of the surface fluxes computed from the 3D mesoscale model in the domain A are indicated during the course of the day. The 'dominant' 1D fluxes are shown in dashed lines, the 'effective' ones in solid lines. One can see that the 'dominant' latent (Fig. 8a) and sensible (Fig. 8b) heat fluxes depart significantly from the reference area-averaged fluxes. Because of the high value of R_{smin}, the 'dominant ' latent heat is underestimated, and the sensible heat flux consequently overestimated. The Bowen ratio prediction with 'effective' properties is significantly improved, although one can note a slight underprediction of the latent heat flux.

Turning our attention to the net radiation (Fig. 8c), the area-averaged flux exhibits some scatter during the morning because of cloudy patches computed with the mesoscale model in this area. Because of a lower predicted surface temperature, the 'effective' net radiation is somewhat higher than the dominant R_n. With 'effective' surface conditions, the prediction of the soil heat flux is particularly improved thanks to the effective value of veg, which allows for a storage of heat into the ground (Fig. 8d). Conversely, the null fraction of bare ground with dominant

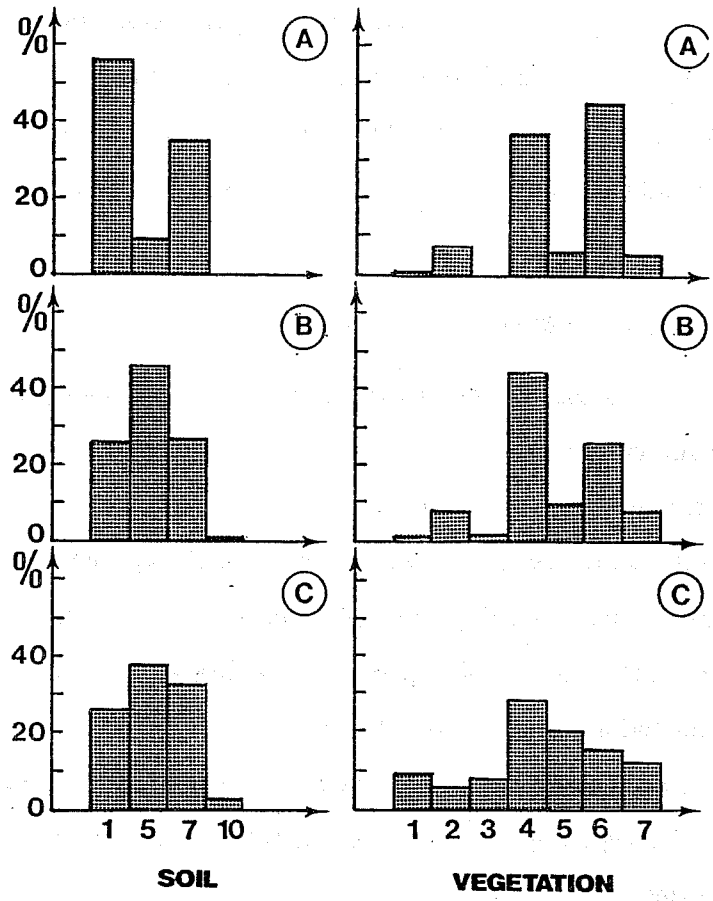

Figure 6: Diagram for the percent of types of soil texture and vegetation found within the mesoscale sub-domains A,B and C (see Fig.2). Classes of vegetation (Phulpin et al., 1989): 1: semi-desert, 2: vineyards, 3: mediterranean vegetation, 4: crops, 5: grasslands, 6: coniferous forest, 7: deciduous forest. The histogram for the vegetation is based on 5824, 38400 and 92414 AVHRR pixels for domains A,B and C, respectively

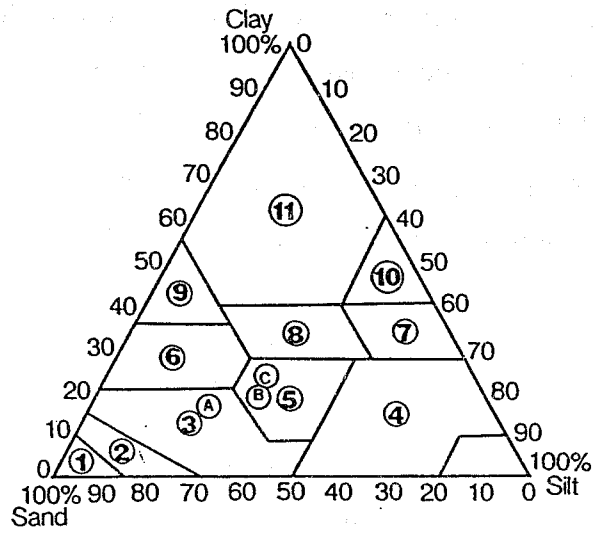

Figure 7: The Clapp and Hornberger's textural triangle. The equivalent soil texture for domains A, B and C are reported.

conditions ($veg \approx 1$) leads to a negligible value for the soil heat flux.

The predictions for the two components of the latent heat flux are given in Fig. 8ef. Once more, better results are obtained with effective surface conditions. Although slightly overestimated during the earliest hours (due to the non cloudy conditions in 1D predictions), the effective transpiration is close to the area-averaged value thanks to the R^e_{smin} value. The dominant ground surface evaporation E_g is very weak , while the effective E_g fits better the 3D results. However, we observe that the effective E_g starts to decrease after $10hours$ and remains lower than the areal evaporation during the rest of the day. It is important to mention that this underprediction of E_g explains the underprediction of the effective total latent heat previously mentioned and is therefore the largest discrepancy observed so far in our comparison between 3D-1D results. We have therefore paid some attention to explain its origin.

In order to examine the influence of the soil texture on the prediction of E_g, we have run various 1D tests with effective properties for the vegetation, but changing the soil texture. Remember that domain A is mainly constituted by the classes 1 and 7 (Fig. 7) and that its equivalent texture is in between classes 3 and 5. In the textural triangle, the soil properties vary highly from sand (1) to silty clay loam (7). For instance the hydraulic conductivity decreases by about two orders of magnitude, with a greater value for sand. Examples of such a variation in soil hydraulic parameters can be seen through coefficients C_{1sat} and C_{2ref} in table 2. Fig. 9 shows the prediction of the effective E_g obtained when considering the textures 1,3,5,7 and the effective one (solid line). The same initial values for the relative soil moisture content (w_g and w_2) have been taken for the various soil types. The test with a sandy soil leads to a strong value of E_g during the whole day as a result of rapid water exchanges between the deep and near-surface reservoir. On the other hand, the low value of the hydraulic conductivity is responsible for the reduced value of E_g after 9 am for silty clay loam. At this stage, it is interesting to note that the standard deviation in the 3D domain during daytime can be mainly explained by the E_g patterns for sand and silty clay loam and that a simple mean of these two contributions is a good approximation of the areal evaporation. On the other hand, results from classes 3 and 5 are close to those obtained with the composite soil texture for domain A. This, indicates that the continuous formulations for soil properties we have adopted seems to work satisfactorily, at least for the case examined. An other very important conclusion is that the departure between the effective and the mean soil evaporation is due to the non linearity in the soil transfers. This example shows clearly some limitation in our aggregation method. May be it is possible to define another averaging method in order to overcome these non-linear effects, for instance by

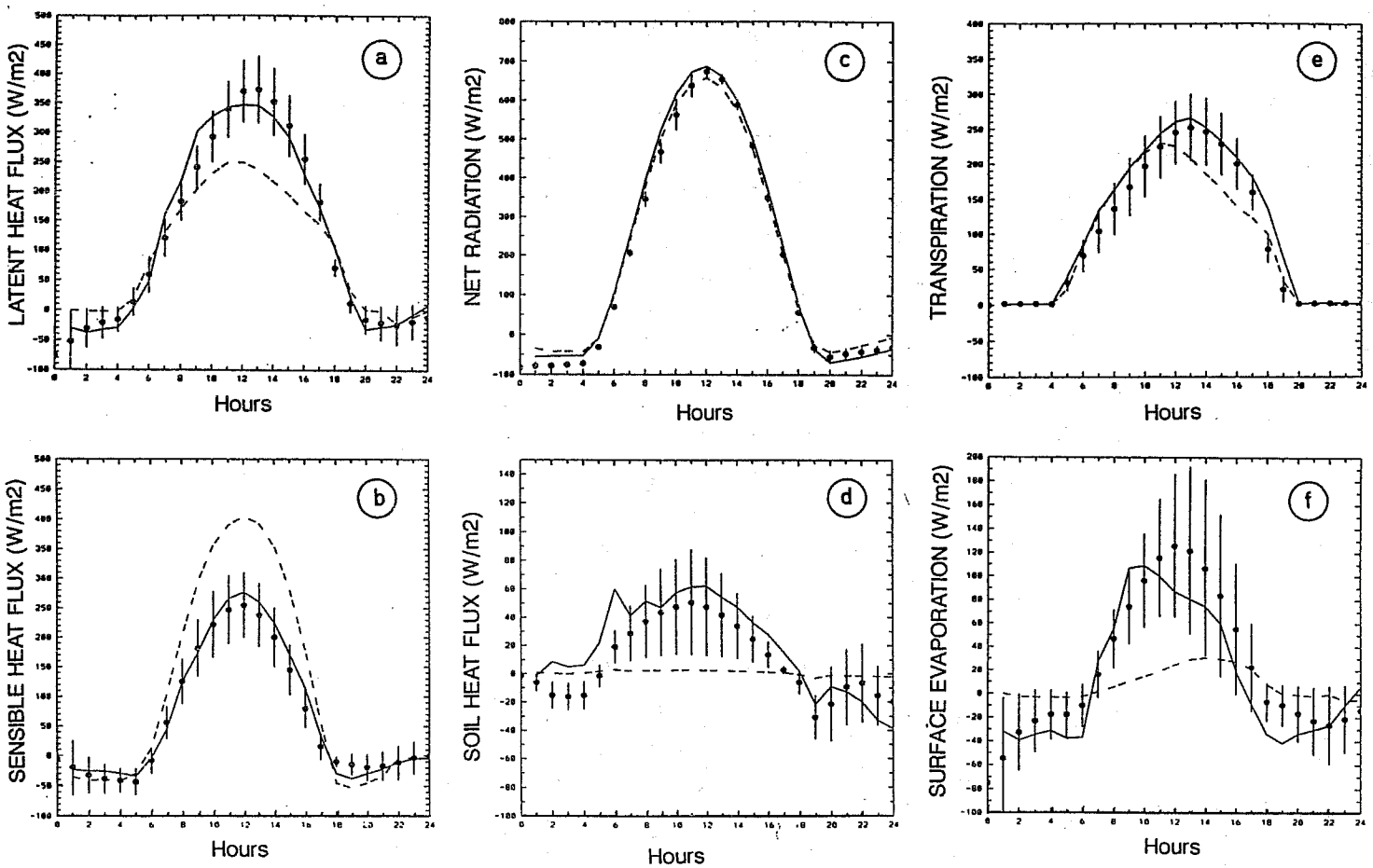

Figure 8: Aggregation results for domain A on 16 june 1986. Comparison between the areally-averaged surface fluxes computed from the 3D model (solid point) and the 1D predictions with dominant (dashed line) or effective (solid line) properties for the soil and the vegetation. The vertical bars represent the standard deviations of the fluxes predicted by the mesoscale model within domain A. Latent heat flux (a), sensible heat flux (b), net radiation (c), soil heat flux (d), plant transpiration (e) and bare soil evaporation (f).

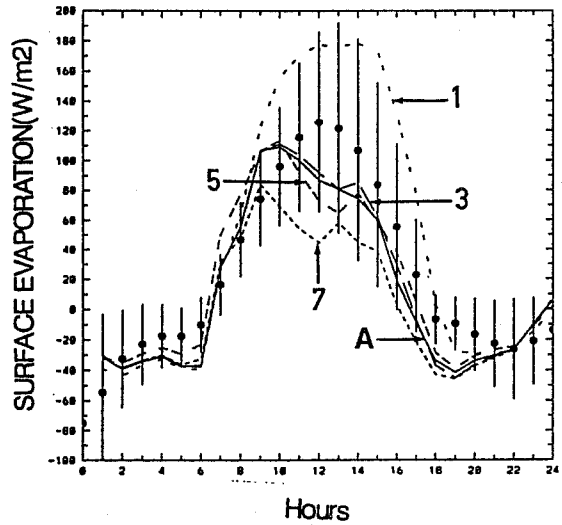

Figure 9: Sensitivity of the effective surface evaporation on the soil texture. The curves correspond to 1D predictions with effective vegetation properties and different soil textures for domain A on 16 june: class 1 (sand), class 7 (silty clay loam), class 3 (sandy loam), class 5 (loam), effective soil properties (solid line). The mean surface evaporation (solid points) and its standard deviation (vertical bars) computed by the mesoscale model are given.

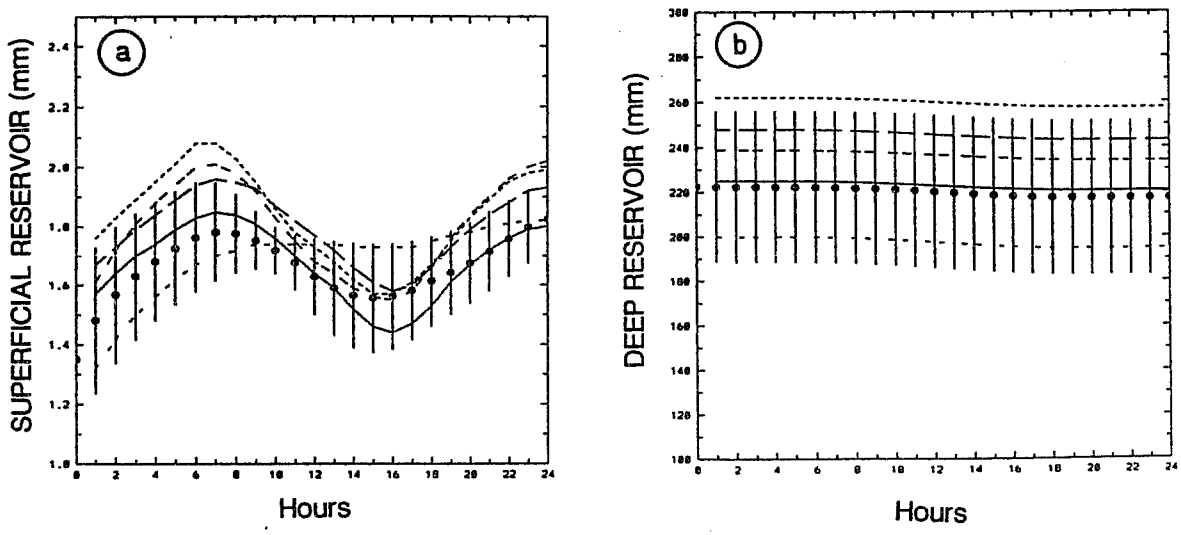

Figure 10: as in fig. 9 but for the near-surface (a) and deep (b) water content.

increasing the weight of the percent of sand in the aggregation process. However, if we turn again to Fig. 8f, the effective surface parameters provide the best estimate for the area flux.

Fig. 10 shows the daily predictions of the superficial (a) and deep (b) water contents integrated over the reservoirs depths $d_1 = 1cm$ and $d_2 = 1m$, respectively. The different initial values of soil moisture are due to the dependence of the saturation volumetric water content w_{sat} on the soil texture. From Fig. 10 it appears clearly that the best estimate of the areally-averaged soil moisture content is performed with the effective soil texture. This, is of particular importance for the total water content since we are mainly interested by the prediction of this quantity over a long-time period, a requirement of GCM's modellers.

• Results in domain B on 16 june 1986

The effective properties of the vegetation for domain B on 16 june do not depart significantly from the dominant properties, except for the fraction of vegetation which is increased from 0.30 to 0.45 (table 4). Effective flux predictions (Fig.11) are slightly better than for dominant fluxes (particularly for E_{tr}) although the same failure as for domain A is observed, e.g. an underestimation of E_g. However, note that the daily variation of effective E_g follows that of dominant E_g thanks to the equivalent soil properties in B, which are close to the hydraulic characteristics of loam, the dominant soil type of the target area. Dominant evaporation is sligtly higher during the day because of the higher fraction of bare ground with dominant surface properties.

• Summary of daily integrations

The results for the different domains and the different days of the study are summarized in table 5. The mean relative daily error for the turbulent fluxes is computed for each case. The relative errors generally exceed 10% when considering dominant properties, reaching large values in some cases. On the other hand, the relative errors are significantly lower with effective properties. The differences between the two methods are less important for domain C because of the smoothed spatial distribution of both soil and vegetation types for the whole simulation domain (see Fig.6). From these tests, it is obvious that aggregation is particularly important when there is a strong spatial contrast in land-use within a large area as illustrated by the bimodal shape of the diagrams in Fig. 6 for domains A and B.

5 A long term integration

Our main objective is to simulate the variation of the total soil water content of the HM86 experimental area for a long time period using the 1D atmospheric column model. Although

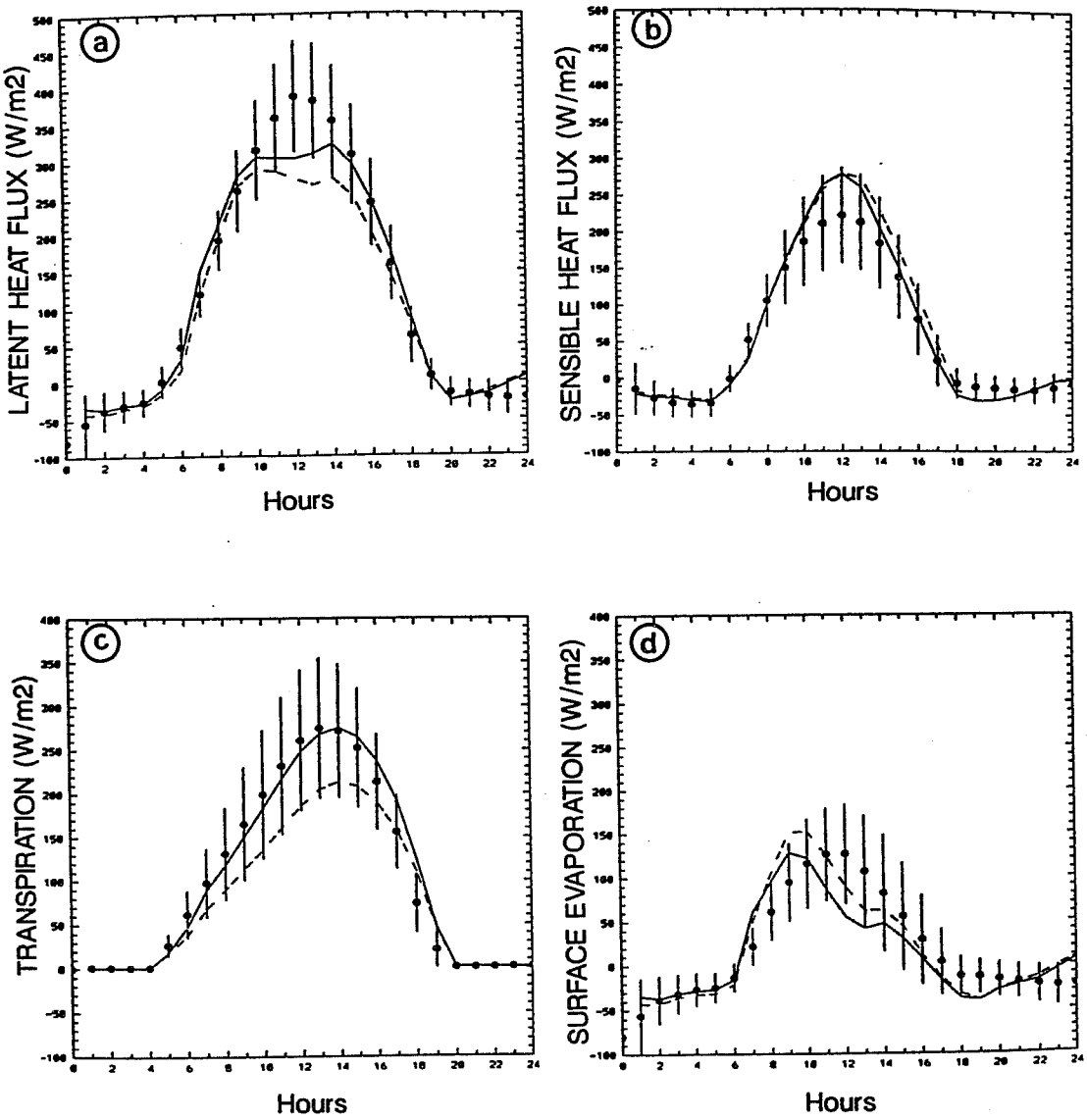

Figure 11: as in Fig. 8 but for domain B on 16 june 1986: latent heat flux (a), sensible heat flux (b), transpiration (c) and surface evaporation (d).

our aggregation rules seem to work satisfactorily for selected daily cycles, it is necessary to check the method over a period long enough in order to allow significant changes in soil water content and vegetation properties. As a first attempt, we performed a 1D integration of 25 days, starting on 16 june. The test conditions are:

(i) Large scale advections are prescribed at each model level from the 1D analyses obtained every 6 hours.

(ii) The atmospheric column is re-initialized every day at 00.00 TU using the 1D analyses. The soil moisture is predicted continuously during the 25 days of the integration.

(iii) Precipitation (Fig. 12) and incoming solar radiation are imposed at each time step from observations taken at a group of surface stations (SAMER stations 3,9,10,11 in Fig. 4)

(iv) The surface properties correspond to either dominant or effective conditions for domain A. In the latter case, the effective properties of the vegetation are interpolated linearly in time between their values calibrated on 16 june and 08 july (table 4).

(v) Initialization of the soil water content: The relative soil water content w_2/w_{sat} is taken equal to 0.50, as observed from neutron soundings at this period of the year (Goutorbe et al. 1989) and assumed in the 3D integration on 16 june. The depth d_2 of the soil is assumed to be $1.00m$. These assumptions lead to a total amount of 225 and $200mm$ of water for the equivalent soil texture and for the sandy soil, respectively.

The prediction of the total water content $w_2 \times d_2$ is given in Fig. 13. The mean value and standard deviation of soil moisture content within domain A computed from the mesoscale model on 16 june and 08 july are indicated. It should be recalled that these water contents in the 3D model were prescribed from observations of the neutron sounding network and that they therefore represent our best approximation to the actual mean value of the soil water during that period. The large standard deviation is explained by i) the two different soil texture present in A (sand and silty clay loam) and ii) differences in soil depths within the area (Mascart et al. 1988).

After 23 days of integration, the predicted soil moisture with effective surface conditions is very close to the 'observed' value on 08 july. On the other hand, with dominant surface properties, the soil water content is significantly lower than the 3D values, consequently to a low initial value. One can observe that the time decrease of soil moisture is lower with dominant conditions because of reduced plant transpiration over the whole period as shown in Fig. 14a. Remember that the same atmospheric forcing is considered for the two integrations and that the differences in soil water predictions are due to differences in predicted latent heat flux. As a first

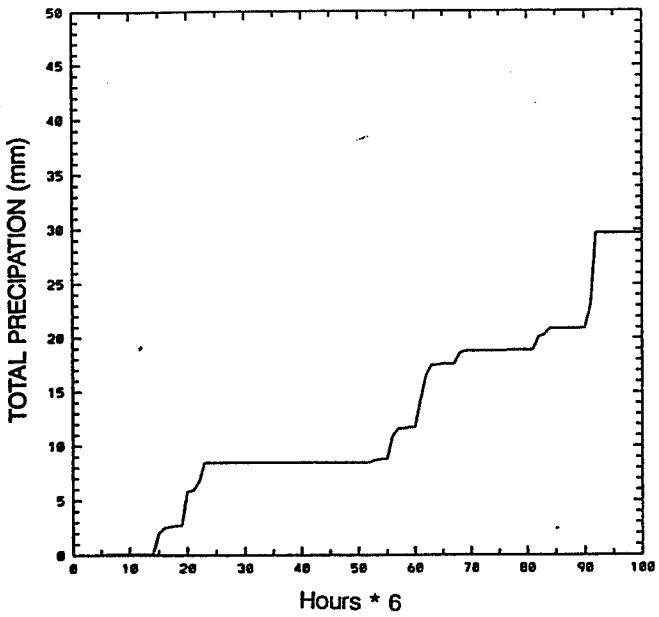

Figure 12: The precipitation forcing prescribed during the 25 days of the 1D integration. This forcing corresponds to measurements at SAMERS stations 3, 9, 10 and 11 (Fig. 4).

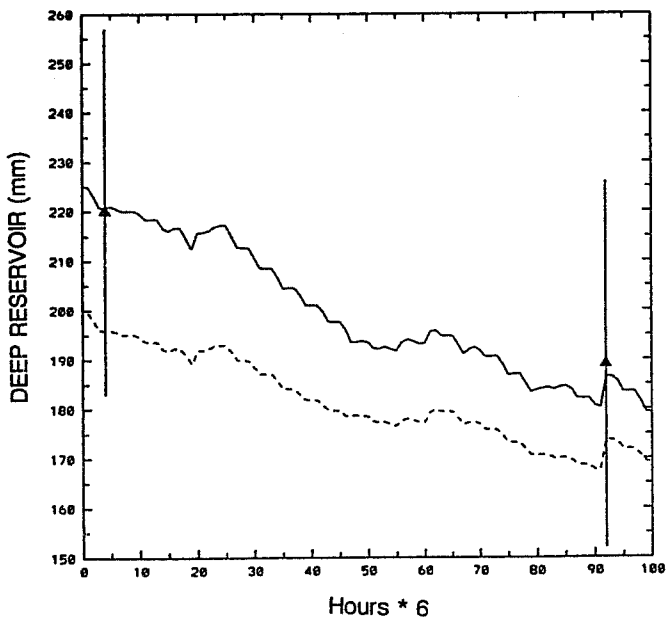

Figure 13: 1D prediction of the time variation of the deep soil water content for 25 days starting on 16 june and lasting on 10 july 1986: effective surface properties (solid line), dominant surface properties (dashed line). The mean values of the soil water content (full triangle) and standard deviation (vertical bars) in the mesoscale domain A on 16 june and 08 july are indicated.

attempt of validation, Fig. 14b proposes a comparison between the total amount of predicted latent heat flux with effective properties and observations at the group of flux stations providing the precipitation and solar radiation forcings. The prediction follows closely the observations for the first 18 days and become then sligtly underestimated.

Although it remains a lot of work to validate our integration, the present result constitutes the ultimate step of our objectives. In the near-future, the following steps will be undertaken:

- Perform an integration for the 70 days of the experiment,
- Constitute a data base for precipitation, radiation and evaporation fields (including the forest site) against which to test the method,
- Validate the prediction of areally-averaged fluxes throughout our 70 days prediction with aircraft estimates available on 25 days (Hildebrand 1988) in domain A and with remotely-sensed surface temperature over the whole area.

6 Conclusions

This paper investigates the problem of aggregation of land-surface properties in a large area comparable in size with a model grid box of a GCM. The study is based upon atmospheric situations encountered during HAPEX-MOBILHY 1986, i. e. moderate plant water stress at the beginning of summer. As a first guess for accounting for spatial variability, it is proposed to estimate effective surface properties describing the spatial distribution of the vegetation and the soil texture within the large area under study. Despite the non-linear dependence of surface fluxes on both vegetation and soil water content, it is found that the effective surface fluxes computed from effective parameters with a 1D column model match the areally-averaged fluxes estimated from 3D mesoscale model results with a relative error less than 10%. On the other hand, fluxes computed with prescribed surface properties associated to the dominant land-use of the large domain depart significantly from the averaged fluxes. For the cases examined, the effects of non-linearity are found to be smaller for the vegetation behaviour than for the soil water tranfers.

The aggregation method has been tested succesfully for a long time period within the context of a 1D GCM grid cell representing the HAPEX-MOBILHY 1986 instrumented area. Given precipitation and solar radiation fluxes, predictions of soil water content and total evaporation for 25 days compare well with observations available within the large area.

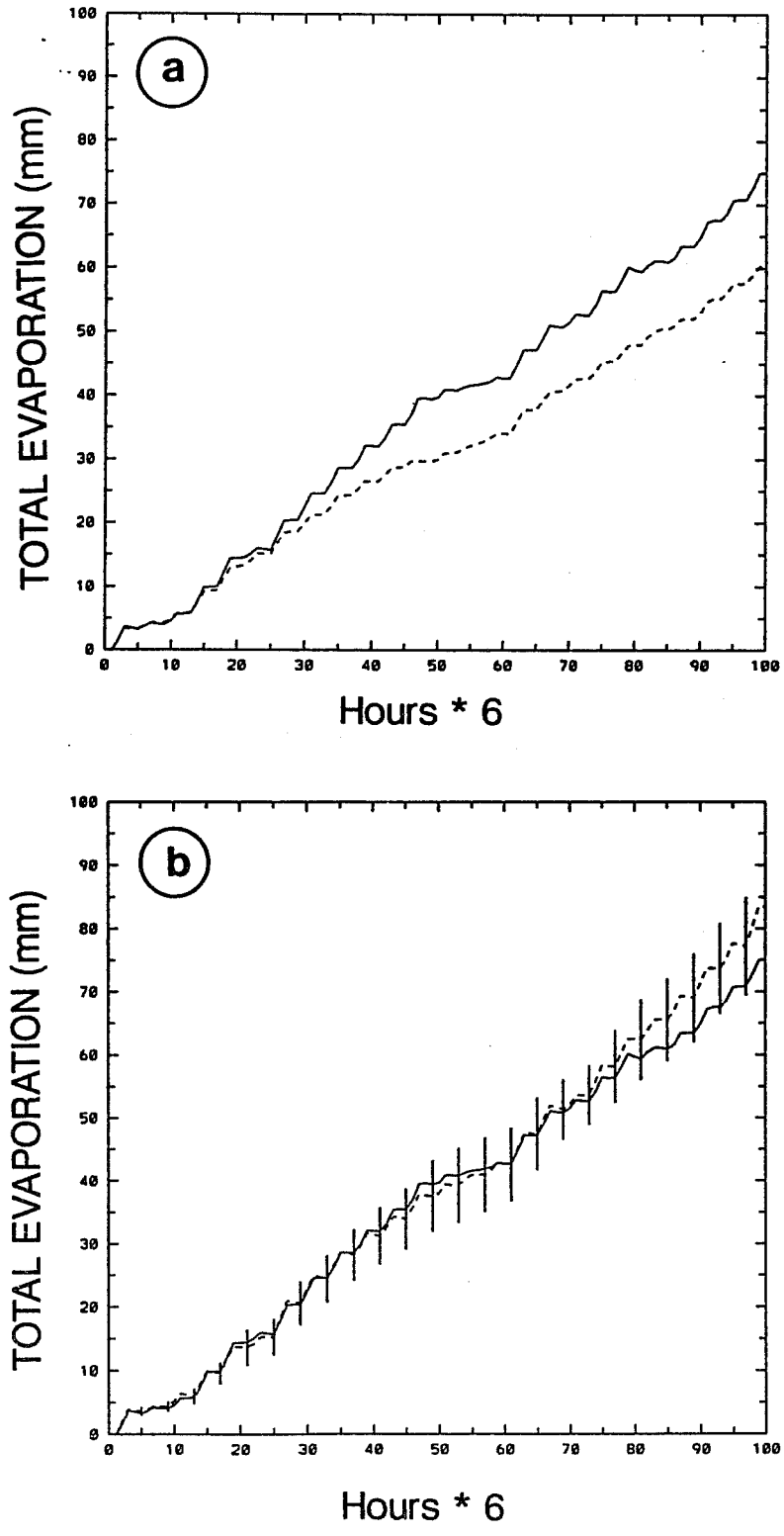

Figure 14: Comparison between 'effective' and 'dominant' latent heat fluxes (a) for the long-term 1D integration. Comparison between the predicted 'effective' latent heat flux and observations at the SAMER stations 3, 9, 10 and 11 (b).

7 Acknowledgments

The authors thank Ph. Bougeault and P. Mascart for the fruitful discussions during the course of this study and their comments on this manuscript.

APPENDIX: Formulation of the land surface parameterization (Noilhan and Planton, 1989)

The model has five pronostic variables: the surface temperature T_s, the mean temperature T_2, the superficial moisture w_g, the bulk soil moisture w_2 and the amount of liquid water W_r retained on the foliage:

$$\frac{\partial T_s}{\partial t} = C_T(R_n - H - LE) - \frac{2\pi}{\tau}(T_s - T_2) \tag{1}$$

$$\frac{\partial T_2}{\partial t} = \frac{1}{\tau}(T_s - T_2) \tag{2}$$

$$\frac{\partial w_g}{\partial t} = \frac{C_1}{\rho_w d_1}(P_g - E_g) - \frac{C_2}{\tau}(w_g - w_{geq}) \qquad 0 \leq w_g \leq w_{sat} \tag{3}$$

$$\frac{\partial w_2}{\partial t} = \frac{1}{\rho_w d_2}(P_g - E_g - E_{tr}) \qquad 0 \leq w_2 \leq w_{sat} \tag{4}$$

$$\frac{\partial W_r}{\partial t} = vegP - E_r \qquad \text{and} \qquad 0 \leq W_r \leq W_{rmax} \tag{5}$$

where τ is a time constant of one day, ρ_w the density of liquid water, d_1 is an arbitrary depth of 1cm, d_2 is the total depth of the soil including the root zone, P is the precipitation rate at the top of the vegetation, P_g is the flux of liquid water reaching the ground surface (non intercepted rainfall plus run-off from canopy), and W_{rmax} is the maximum value of W_r , expressed as Dickinson's proposal (1984): $W_{rmax} = (0.2)\ veg\ LAI \qquad (mm)$

The hydric coefficients C_1 and C_2, and the equilibrium value w_{geq} have been calibrated using the results of a detailed soil model. They are expressed as functions of soil texture and soil moisture by:

$$C_1 = C_{1sat}\left(\frac{w_{sat}}{w_g}\right)^{b/2+1} \tag{6}$$

$$C_2 = C_{2ref}\left(\frac{w_2}{w_{sat} - w_2 + w_f}\right) \tag{7}$$

$$\left(\frac{w_{geq}}{w_{sat}}\right) = \frac{w_2}{w_{sat}} - a\left(\frac{w_2}{w_{sat}}\right)^p\left(1 - \frac{w_2}{w_{sat}}\right)^{8p} \tag{8}$$

The values of the numerical coefficients a, b, p, w_f, and of the saturated volumetric moisture content w_{sat}, which only depend on soil texture, are given in table 2.

The coefficient C_T combines the thermal inertia of the soil C_G and of the vegetation C_V. It is expressed as:

$$C_T = 1/(\frac{1 - veg}{C_G} + \frac{veg}{C_V})$$

with $C_G = C_{gsat} \frac{w_{sat}}{w_2} \frac{b}{2 \ln 10}$ and $C_V = 10^{-3} K m^2 J^{-1}$

The turbulent fluxes in the surface boundary layer are computed by means of the classical surface boundary layer formulation. The sensible heat flux is written:

$$H = \rho_a \quad C_p \quad \frac{T_s - T_a}{R_a}$$

where ρ_a is the air density, C_p is the specific heat of air, T_a is the air temperature at the atmospheric height z_a, and R_a is the aerodynamic resistance, which depends on wind speed and on a drag coefficient computed from Louis et al. (1981).

Separate calculations are made for evaporation E_r from wet parts of the canopy, transpiration E_{tr} from dry parts, and evaporation E_g from the soil. The total flux E is calculated by weighting those estimates by the fractional area occupied by each, based on the canopy cover, veg, and an estimate of δ the wet fraction of the canopy capacity (Deardorff 1978).

The ground relative humidity, related to the superficial volumetric moisture content is given by:

$$Hu = \begin{cases} 0.5 \quad (1 - \cos(\quad \pi \frac{w_g}{w_{fc}})) & \text{if} \quad w_g \leq w_{fc} \\ 1, & \text{otherwise} \end{cases}$$

The surface resistance R_s is made dependent both upon atmospheric factors (F_1, F_3, F_4) and upon total available water in the soil (F_2) :

$$R_s = \frac{R_{smin}}{LAI \quad F_1 \quad F_2 \quad F_3 \quad F_4}$$

where the limiting factors F_1, F_2, F_3, F_4 are computed by:

$$F_1 = \frac{f + R_{smin}/R_{smax}}{1 + f} \tag{9}$$

$$F_2 = \frac{w_2 - w_{wilt}}{w_{fc} - w_{wilt}} \quad and \quad 0 \leq F_2 \leq 1 \tag{10}$$

$$F_3 = 1 - \alpha(q_{sat}(T_a) - q_a) \tag{11}$$

$$F_4 = 1 - 1.6 \times 10^{-3}(T_a - 298.15)^2 \tag{12}$$

where the dimensionless term f represents the incoming photosynthetically active radiation on the foliage, normalized by a species-dependent threshold value ; α is a species dependent parameter (see Jacquemin and Noilhan, 1990) and R_{smax} is arbitrarily set to $5000 s/m$. In this study, the values of w_{wilt} and w_{fc} are equal to $0.3 w_{sat}$ and $0.6 w_{sat}$, respectively.

Primary Parameters	Secondary Parameters	Notation	Units
Dominant type of soil texture	Saturated volumetric moisture	w_{sat}	m^3m^{-3}
	Wilting point volumetric moisture	w_{wilt}	m^3m^{-3}
	Slope of the retention curve	b	-
	Saturated soil thermal coefficient	C_{Gsat}	Km^2J^{-1}
	Value of C_1 at saturation	C_{1sat}	-
	Value of C_2 for $w_2 = 0.5w_{sat}$	C_{2ref}	-
	Coefficients of w_{geq} formulation	a, p	-
Depth of soil	Depth of soil	d_2	m
Dominant type of vegetation	Fraction of vegetation	veg	-
	Minimum surface resistance	R_{smin}	sm^{-1}
	Leaf area index	LAI	m^2m^{-2}
	Roughness length	z_0	m
Albedo	Albedo	α	-
	Emissivity	ϵ	-

Table 1: A list of parameters in the NP89 surface model.

Soil texture	w_{sat}	b	c_{gsat}	p	a	C_{2ref}	C_{1sat}
Sand	0.395	4.05	3.222	4	0.387	3.9	0.082
Loamy sand	0.410	4.38	3.057	4	0.404	3.7	0.098
Sandy loam	0.435	4.90	3.560	4	0.219	1.8	0.132
Silt loam	0.485	5.30	4.418	6	0.105	0.8	0.153
Loam	0.451	5.39	4.111	6	0.148	0.8	0.191
Sandy clay loam	0.420	7.12	3.670	6	0.135	0.8	0.213
Silty clay loam	0.477	7.75	3.593	8	0.127	0.4	0.385
Clay loam	0.476	8.52	3.995	10	0.084	0.6	0.227
Sandy clay	0.426	10.4	3.058	8	0.139	0.3	0.421
Silty clay	0.482	10.4	3.729	10	0.075	0.3	0.375
Clay	0.482	11.4	3.600	12	0.083	0.3	0.342

Table 2: Values of the soil parameters according to the textural classification of Clapp and Hornberger (1978) and Noilhan and PLanton 's (1989) calibration: b is the slope of the retention curve, the saturation moisture content w_{sat} is in m^3/m^3, C_{gsat} is in $10^{-6}Km^2J^{-1}$ and all other coefficients are dimensionless.

Dominant vegetation type	Class	veg	LAI	z_0	R_{smin}
Desert	1	0.10	0.1	0.15	999
Orchards and Vineyards	2	0.40	1.0	0.15	80
Mediterranean vegetation	3	0.40	1.0	0.15	80
Crops	4	0.30	1.0	0.15	40
Grasslands	5	0.60	1.5	0.15	40
Coniferous forest	6	0.99	2.3	1.0	150
Deciduous forest	7	0.90	3.0	1.0	100

16 JUNE 1986

Dominant vegetation type	Class	veg	LAI	z_0	R_{smin}
Desert	1	0.10	0.1	0.15	999
Orchards and Vineyards	2	0.50	1.0	0.15	80
Mediterranean vegetation	3	0.50	1.0	0.15	80
Crops	4	0.70	2.0	0.15	40
Grasslands	5	0.70	2.0	0.15	40
Coniferous forest	6	0.99	2.3	1.0	150
Deciduous forest	7	0.90	3.0	1.0	100

08 JULY 1986

Table 3: The values of the parameters assigned to each type of dominant vegetation on 16 june and 08 july 1986.

test	day	domain	soil	vegetation	veg	R_{smin} (s/m)	LAI (m2/m2)	Z_o (m)
1	16 june	A	dominant (sand)	dominant (forest)	0.99	150	2.3	1.00
2	16 june	A	effective	effective	0.64	66	1.7	0.38
3	08 july	A	dominant (sand)	dominant (forest)	0.99	150	2.3	1.00
4	08 july	A	effective	effective	0.82	66	2.1	0.38
5	16 june	B	dominant (loam)	dominant (crops)	0.30	40	1.0	0.15
6	16 june	B	effective	effective	0.45	59	1.5	0.25
7	16 june	C	dominant (loam)	dominant (crops)	0.30	40	1.0	0.15
8	16 june	C	effective	effective	0.57	75	1.15	0.13

Table 4: Summary of surface conditions for daily 1D integrations performed for domains A,B and C on 16 june and 08 july 1986.

day	domain	soil	vegetation	$\frac{(\overline{LE_{1D}} - \overline{LE_{3D}})}{\overline{LE_{3D}}}$	$\frac{(\overline{H_{1D}} - \overline{H_{3D}})}{\overline{H_{3D}}}$
16 june	A	dominant (sand)	dominant (forest)	0.19	0.76
16 june	A	effective	effective	-0.02	-0.09
08 july	A	dominant (sand)	dominant (forest)	0.33	0.45
08 july	A	effective	effective	0.02	0.02
16 june	B	dominant (loam)	dominant (crops)	0.17	-0.21
16 june	B	effective	effective	0.04	-0.12
16 june	C	dominant (loam)	dominant (crops)	0.10	0.10
16 june	C	effective	effective	-0.07	0.01

Table 5: Comparison between the mean daily relative error for latent and sensible heat fluxes computed with **effective** or **dominant** surface properties (see Table 4)

References

André, J.C., P. Bougeault, J.F. Mahfouf, P. Mascart, J. Noilhan, and J.P. Pinty, 1989: Impact of forest on mesoscale meteorology. *Phil. Trans. R. Soc. Lond. B*, **324**, 407–422.

André, J.C., J.P. Goutorbe, A. Perrier, F. Becker, P. Bessemoulin, P. Bougeault, Y. Brunet, W. Brutsaert, T. Carlson, R. Cuenca, J. Gash, J. Gelpe, P. Hildebrand, J.P. Lagouarde, C. Lloyd, L. Mahrt, P. Mascart, C. Mazaudier, J. Noilhan, C. Ottlé, M. Payen, T. Phulpin, R. Stull, J. Shuttleworth, T. Schmugge, O. Taconet, C. Tarrieu, R.M. Thépenier, C. Valencogne, D. Vidal-Madjar, and A. Weill, 1988: Evaporation over land surfaces: first results from HAPEX-MOBILHY special observing period. *Annales Geophysicae*, **6 (5)**, 477–492.

Attie, J.L., 1990: *Etude des processus d'évaporation des surfaces continentales.* Technical Report, DEA, CNRM, 31057 Toulouse, France.

Avissar, R. and R.A. Pielke, 1989: A parameterization of heterogeneous land surfaces for atmospheric numerical models and its impact on regional meteorology. *Mon. Wea. Rev.*, **117**, 2113–2136.

Blyth, E., A.J. Dolman, and N. Wood, 1991: Calculation of the effective surface resistance to evaporation to heterogeneous terrain. . (in prep.).

Bougeault, Ph., B. Bret, P. Lacarrère, and J. Noilhan, 1991b: An experiment with an advanced surface parameterization in a meso-beta-model. part II: the 16 june 1986 simulation. *Mon. Wea. Rev.*, **119**, (10), 2374–2392.

Bougeault, Ph., J. Noilhan, P. Lacarrère, and P. Mascart, 1991a: An experiment with an advanced surface parameterization in a meso-beta-model. part I: implementation. *Mon. Wea. Rev.*, **119**, (10), 2358–2373.

Clapp, R.B. and G.M. Hornberger, 1978: Empirical equations for some hydraulic properties. *Water Resour. Res.*, **14**, 601–604.

Claussen, M., 1991: Estimation of areally-averaged surface fluxes. *Bound.-Layer Meteor.*, **54**, 387–410.

Cosby, B.J., G.M. Hornberger, R.B. Clapp, and T.R. Ginn, 1984: A statistical exploration of the relationships of soil moisture characteristics to the physical properties of soils. *Water Resour. Res.*, **20**, (6), 682–690.

Deardorff, J.W., 1978: Efficient prediction of ground temperature and moisture with inclusion of a layer of vegetation. *J. Geophys. Res.*, **83**, 1889–1903.

Dickinson, R.E. *Modeling evapotranspiration for three-dimensional global climate models*, pages 58–72. Volume 29 of *Climate Processes and Climate sensitivity*, American Geophysical Union, 1984. Geophys. Monog.

Dolman, A.J., 1991: A note on areally-averaged evaporation and the value of the effective surface conductance. *J. of Hydrology*, . (in prep.).

Gash, J.H.C., W.J. Shuttleworth, C.R. Lloyd, J.C. André andJ.P. Goutorbe, and J. Gelpe, 1989: Micrometeorological measurements in Les LANDES forest during HAPEX-MOBILHY. *Agri. Forest Mereorol.*, **46**, 131–147.

Germain, M.J., 1990: *Validation d'une paramétrisation des échanges de surface sur differents types de végétation.* Technical Report, CNRM/EERM.

Giordani, H., 1991: *Représentation des échanges de surface dans les modèles météorologiques.* Technical Report, CNRM, 31057, Toulouse, France.

Goutorbe, J.P., J. Noilhan, C. Valancogne, and R.H. Cuenca, 1989: Soil moisture variations during HAPEX-MOBILHY. *Annales Geophysicae*, **7** (4), 415–426.

Hildebrand, P., 1988: *Flux and sounding data from the NCAR King Air aircraft during HAPEX.* Technical Report 319, NCAR.

Jacquemin, B. and J. Noilhan, 1990: Sensitivity study and validation of a land surface parameterization using the HAPEX-MOBILHY data set. *Bound.-Layer Meteor.*, **52**, 93–134.

Mahfouf, J.F., 1990: A numerical simulation of the surface moisture budget during HAPEX-MOBILHY. *Bound.-Layer Meteor.*, **53**, 201–222.

Mahfouf, J.F. and B. Jacquemin, 1989: A study of rainfall interception using a land surface parameterization for mesoscale meteorological models. *J. Appl. Meteor.*, **28**, 1282–1302.

Mahfouf, J.F. and J. Noilhan, 1991: Comparative study of various formulations of evaporation from bare soil using in-situ data. *J. Appl. Meteor.*, **30**, (9), 1354–1365.

Mahfouf, J.F., E. Richard, and P. Mascart, 1987: The influence of soil and vegetation on the development of mesoscale circulations. *J. Climate Appl. Meteor.*, **26**, 1483–1495.

Mascart, P., J. Gelpe, and J.P. Pinty, 1988: *Etude des caractéristiques des sols dans la zone Hapex-Mobilhy 86.* Technical Report 95, OPGC.

Mascart, P., O. Taconet, J. P. Pinty, and M. Ben Mehrez, 1991: Canopy resistance formulation and its effect in mesoscale model: a HAPEX perspective. *Agri. and For. Meteor.*, **54**, 319–351.

Mason, P.J., 1988: The formation of areally-averaged roughness lengths. *Quart. J. Roy. Meteor. Soc.*, **114**, 399–420.

Noilhan, J., J.P. Jullien, P. Lacarrere, T. Phulpin, and M. Stoll, 1991: Quelques exemples d'utilisation des données satellitaires pour la modélisation atmosphériques à moyenne échelle. (use of satellite data in mesoscale atmospheric modelling). In *Physical Measurements and signatures in remote sensing*, pages 541–546, ESA SP-319.

Noilhan, J., P. Lacarrère, and Ph. Bougeault, 1991: An experiment with an advanced surface parameterization in a meso-beta-model. part III: comparison with the HAPEX-MOBILHY data set. *Mon. Wea. Rev.*, **119**, (10), 2393–2413.

Noilhan, J. and S. Planton, 1989: A simple parameterization of land surface processes for meteorological models. *Mon. Wea. Rev.*, **117**, 536–549.

Phulpin, T., J.P. Jullien, and D. Lasselin, 1989: AVHRR Data processing to study the surface canopies in temperate regions. First results of HAPEX. *Int. J. Remote-Sensing*, **10**, 869–884.

Phulpin, T. and J. Noilhan, 1989: Use of AVHRR and METEOSAT data for the determination of land surface parameters. *Adv. Space Res.*, **9**, 269–274.

Pinty, J.P., 1991: *Analyse et simulation de la couche limite planétaire pendant l'expérience Hapex-Mobilhy avec un modèle numérique 3-D à méso-échelle incluant les effets de la végétation.* PhD thesis, University of Clermont-Ferrand.

Pinty, J.P., P. Mascart, E. Richard, and R. Rosset, 1989: An investigation of mesoscale flows induced by vegetation inhomogeneities using an evapotranspiration model calibrated against HAPEX-MOBILHY data. *J. Appl. Meteor.*, **28**, 976–992.

Shuttleworth, W.J., 1988: Macrohydrology: the new challenge for process hydrology. *J. of Hydrology*, **100**, 31–56.